IOP Conf. Series: Materials Science and Engineering **84** (2015) 012018 doi:10.1088/1757-899X/84/1/012018

The effects of natural, forced and thermoelectric magnetohydrodynamic convection during the solidification of thin sample alloys

A. Kao[1], N. Shevchenko[2], O. Roshchupinka[2], S. Eckert[2], K. Pericleous[1]
[1]Centre of Numerical Modelling and Process Analysis, University of Greenwich, Park Row, London, SE10 9LS
[2]Helmholtz-Zentrum Dresden-Rossendorf, Institue of Fluid Dynamics, P.O. Box 510119, 01314 Dresden, Germany

E-mail: a.kao@greenwich.ac.uk

Abstract. Using a fully coupled transient 3-dimensional numerical model, the effects of convection on the microstructural evolution of a thin sample of Ga-In25%wt. was predicted. The effects of natural convection, forced convection and thermoelectric magnetohydrodynamics were investigated numerically. A comparison of the numerical results is made to experimental results for natural convection and forced convection. In the case of natural convection, density variations within the liquid cause plumes of solute to be ejected into the bulk. When forced convection is applied observed effects include the suppression of solute plumes, preferential secondary arm growth and an increase in primary arm spacing. These effects were observed both numerically and experimentally. By applying an external magnetic field inter-dendritic flow is generated by thermoelectrically induced Lorentz forces, while bulk flow experiences an electromagnetic damping force. The former causes preferential secondary growth, while the latter slows the formation of solute plumes. This work highlights that the application of external forces can be a valuable tool for tailoring the microstructure and ultimately the macroscopic material properties.

1. Introduction

Convective transport of solute is known to have a dramatic effect on the evolution of the underlying microstructure during solidification. In many cases the fluid flow is an inherent part of the process, for example, natural convection is significant in alloys that have relatively large density differences between the various components causing plumes of solute to be ejected back into the melt. These can lead to preferential flow channels (or chimneys) and ultimately the formation of freckles. This phenomenon is common in Nickel based super alloys which are widely used in the manufacturing of gas turbine blades [1-3]. Performing direct *in situ* experimental studies on Nickel based super alloys is very difficult due to the high solidification temperature. An alternative system to study the underlying mechanism is the Gallium-Indium system, which is liquid at room temperature and easy to handle. Furthermore, due to a relatively large density difference between Gallium and Indium, the system exhibits similar flow behaviour to Nickel based super alloys. An *in situ* radiographic technique has been developed by Eckert and co-workers [4-6]. In this work the same experimental technique is used to validate the numerical studies.

Numerical models have been used to investigate the formation of freckles in castings [7-9], however they have primarily focused on the effects of natural convection. This work focuses on the introduction of external forces in the liquid to modify the fluid dynamics. The first is the application of a magnetic wheel, which generates an alternating magnetic field providing conditions analogous to forced convection close to the solidification front. The second is the application of a static external magnetic field, which has two effects, the first is electromagnetic damping and the second is thermoelectric magnetohydrodynamics (TEMHD). The latter is caused by the interaction with

thermoelectric currents localised to the solidification front giving a resultant Lorentz force, hence driving fluid flow. In this work a fully coupled transient 3-dimensional numerical model was applied to each of these cases. The model uses an Enthalpy based method originally developed by Voller [10]. The Enthalpy based method is a level set method that uses an iterative finite difference scheme to solve the Gibbs-Thompson condition and conservation of enthalpy. This method has been extended by Kao *et al*. [11,12] into 3-dimensions and to include fluid flow and electromagnetics. It has been used to investigate TEMHD to control microstructure evolution [13], the role of secondary arms in TEMHD [14] and the effect of slow rotating fields [15].

Understanding the effect of external forces on microstructure is fundamentally important for both the generation of new materials and improving current techniques. The capability to predict the outcome of microstructural modifications due to externally applied forces will allow for macroscopic material properties to be tailored by selective design of these forces.

2. Governing Equations

The evolution of the microstructure is modelled using an enthalpy-based method. The volumetric enthalpy H is defined as the sum of sensible latent heats

$$H = c_p T + fL \tag{1}$$

where, c_p is the volumetric specific heat capacity and L is the volumetric latent heat of fusion. For binary alloys the concentration potential V in terms of the solute concentration C and partitioning coefficient k is defined as

$$V = \frac{C}{f(1-k)+k}. \tag{2}$$

The interfacial temperature (T^i) is given by the Gibbs-Thompson condition

$$T^i = T_m - \frac{\gamma(\theta,\phi)}{L} T_m \kappa - m\left(C_0 - C_l^i\right) \tag{3}$$

where T_m is the melting temperature, $\gamma(\theta,\phi)$ is the surface energy, κ the curvature, m the liquidus slope, C_0 the bulk solute concentration and C_l^i the liquid solute concentration at the interface. Due to the low thermal Péclet number (Pe $<10^{-2}$) and large time scales involved, the thermal field can be assumed to be at a steady state and diffusion dominated. Consequently the thermal field at a given time is known explicitly from the imposed thermal gradient, G and nucleation temperature, T_0. However, due to a large Lewis number, Le = 10000, mass transport needs to be solved by

$$\frac{dC}{dt} = \nabla \cdot \left(D_l \nabla V\right) - \nabla \cdot \left(\mathbf{u} V\right) \tag{4}$$

where D_l is the liquid mass diffusivity. In the solid the Scheil assumption, $D_s = 0$ is used.
Due to the low Reynolds number encountered on the scale of microstructures and thin sample experiments, a simplified form of the Navier-Stokes equation is used, representing Stokes flow

$$\rho \frac{d\mathbf{u}}{dt} = -\nabla p + \mu \nabla^2 \mathbf{u} + \mathbf{F} \tag{5}$$

where ρ is the density, **u** the velocity, p the pressure, μ the dynamic viscosity and **F** is the sum of all the body forces. Conservation of mass for incompressible flow gives

$$\nabla \cdot \mathbf{u} = 0 . \tag{7}$$

For natural convection, the body force **F** in (5) is given by

$$\mathbf{F}_{NC} = \rho \mathbf{g} f \beta (C - C_0) \tag{8}$$

where β is the compositional expansion coefficient and **g** is the gravitational acceleration. In the case of forced convection, $\mathbf{F}_{FC}$ is assumed to be a constant body force acting over the entire domain. Furthermore, due to the relatively small thickness, W of thin samples and low Reynolds number the flow between the plates can be assumed to be Poiseuille flow. By selecting a characteristic bulk mean velocity $\bar{\mathbf{u}}$ the body force can be calculated from

$$\mathbf{F}_{FC} = \frac{\bar{\mathbf{u}} \mu}{2W^2} . \tag{9}$$

For TEMHD, the current density, **J** is given by a generalised form of Ohm's law including an extra term accounting for thermoelectric currents [16]

$$\frac{\mathbf{J}}{\sigma} = \mathbf{E} - S \nabla T + \mathbf{u} \times \mathbf{B} \tag{10}$$

where σ is the electrical conductivity, **E** the electric field, S the Seebeck coefficient and **B** the DC magnetic field. Conservation of charge gives

$$\nabla \cdot \mathbf{J} = 0 . \tag{11}$$

The thermoelectric currents interact with the magnetic field generating a Lorentz force given by

$$\mathbf{F}_{TE} = \mathbf{J} \times \mathbf{B} . \tag{12}$$

3. Problem Description

Solidification of Ga-In25wt%. alloy in a Hele-Shaw cell with dimensions 25 X 35 X 0.15mm^3 was observed by X-ray radiography. The Hele-Shaw cell was cooled at the bottom by a Peltier cooler at a rate of 0.01K/s. An electric heater at the top with variable heating power was applied to maintain a thermal gradient of 1K/mm over the entire cell. A magnetic wheel was applied at the top of the cell to provide forced convection conditions. The sample is cooled from a molten state and at time t = 0s nucleation occurs and solidification of the microstructure propagates from the base of the sample to the top. A schematic of the experimental setup is given in figure 1.

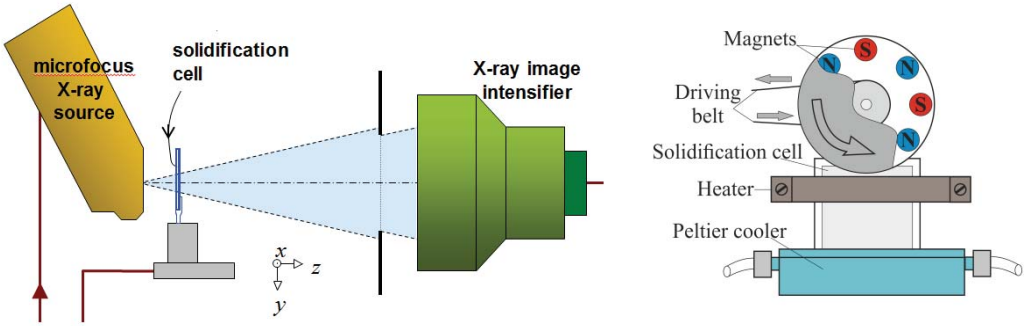

Figure 1. Experimental setup. Left: X-ray radiography system. Right: Hele-Shaw solidification cell with electric heater, Peltier cooler and magnetic wheel.

The numerical model simulates a 5 X 5 X 0.1mm^3 region of the solidification cell. The computational grid comprises cubes with a length of 5μm. In the latter stages of solidification, when the interface reaches 5/8ths of the length of the domain, the domain begins to move at the interface velocity tracking the tips. Table 1 describes the boundary conditions for concentration, temperature, pressure, velocity and current. The location of the faces is shown in figure 2 which gives the relative size of the numerical domain. Periodic boundary conditions are applied on the *x* faces normal to the thermal gradient representing an infinitely wide sample.

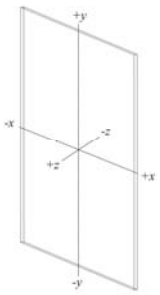

Figure 2. Computational domain.

Table 1. Boundary conditions for numerical model

Face	C	T	p	**u**	**J**
-*x*	Periodic				
+*x*	Periodic				
-*y*	$\frac{dC}{dy}=0$	$T=T_C$	$\frac{dp}{dy}=0$	$\frac{du_x}{dy}=u_y=\frac{du_z}{dy}=0$	$\nabla\cdot\mathbf{J}=0$
+*y*	$C=C_0$	$T=T_H$	$p=0$	$\frac{du_x}{dy}=\frac{du_y}{dy}=\frac{du_z}{dy}=0$	$\mathbf{J}=0$
-*z*	$\frac{dC}{dz}=0$	$\frac{dT}{dz}=0$	$\frac{dp}{dz}=0$	$u_x=u_y=u_z=0$	$\frac{d\Psi}{dz}=0$
+*z*	$\frac{dC}{dz}=0$	$\frac{dT}{dz}=0$	$\frac{dp}{dz}=0$	$u_x=u_y=u_z=0$	$\frac{d\Psi}{dz}=0$

The numerical model assumes that the crystallographic orientation is parallel to the thermal gradient. However, the orientation cannot be controlled experimentally. The experimental results presented below are for cases were nucleation was approximately parallel to the thermal gradient. The material properties used in the numerical model are given in Table 2.

Table 2. Material properties used in the numerical model

c_p	2.38 X 10^6	J/m^3/K	ρ	6250	Kg/m^3
L	4.2 X 10^8	J/m^3	μ	1.25 X 10^{-3}	Pas
k	0.5	-	β	1.66 X 10^{-3}	Wt%$^{-1}$
m	1.8	K/wt%	S	2.5 X 10^{-7}	V/K
D_l	1.2 X 10^{-9}	m^2/s	σ	3.0 X 10^6	S/m

4. Results

4.1 Natural convection

This section investigates the evolution of the microstructure from natural convection only. The absence of forced convection or an external magnetic field provides a control solution that is used to compare against cases when additional external forcing is applied.

Numerical and experimental results of the time evolution of the microstructure are given in figure 3. The figure shows numerical results for the velocity and both numerical and experimental results for the solute concentration. The numerical results show that during the early stages of growth convective rolls form around the nucleation site. Upward flow directed toward the bulk melt, forms plumes of enriched liquid stunting local growth, while downward flow directed onto the solidification front, transports bulk material encouraging growth. The plumes are sustained by drawing enriched solute from the inter-dendritic network. However, as the primary arms grow into the downward flow and the inter-dendritic porosity decreases the convective rolls destabilise and the plumes migrate along the solidification front to the furthest extent of solidification. The upward flow stunts growth at this new location, but the downward flow, now directed toward the previously stunted regions, encourages growth. This transient process then repeats itself. The experimental results show a similar transient behaviour of the plume and there is a reasonable agreement between the predicted primary arm spacing and concentration profiles.

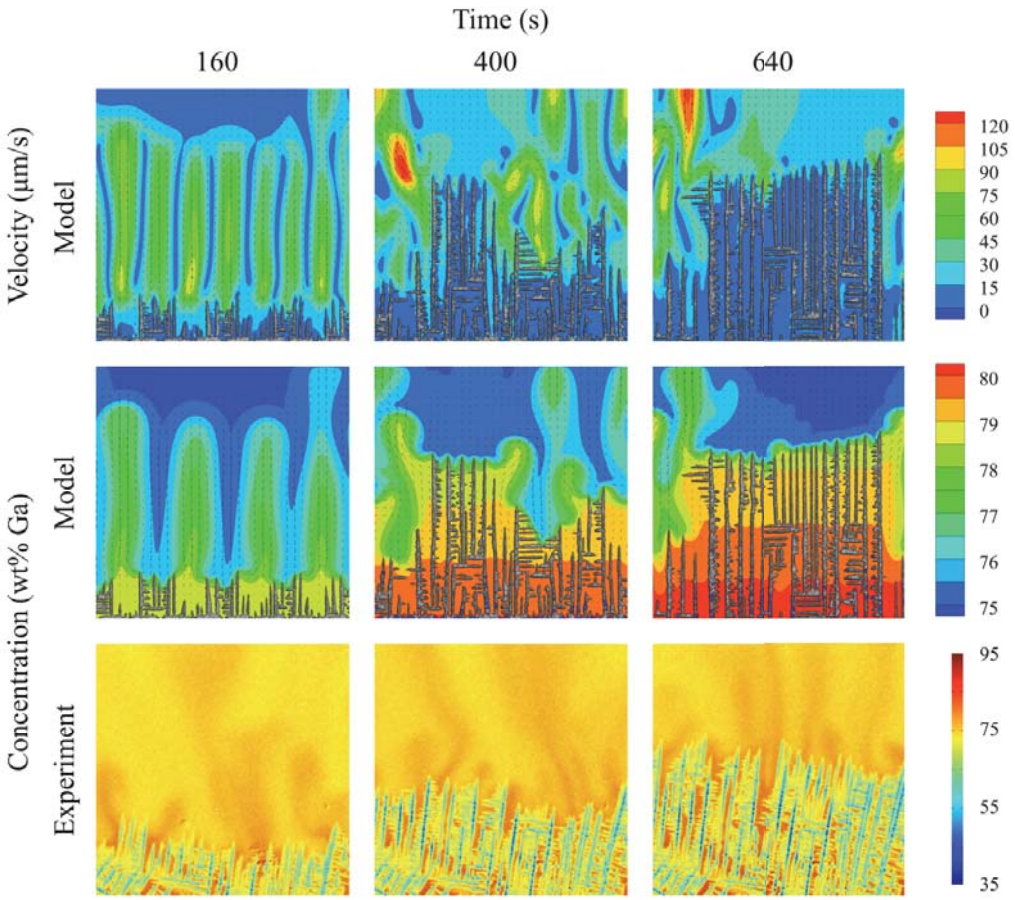

Figure 3. Transient evolution of microstructure under the influence of natural convection. Top: numerical model flow velocity. Middle: numerical model solute concentration. Bottom: experimental solute concentration

4.2 Forced convection

This section introduces an additional body force in the liquid directed perpendicular to the direction of solidification representing forced convection. Experimentally, the rotation of the magnetic wheel introduces electromagnetic forces with greatest intensity at the top of the sample. Further down the sample a pressure gradient forms across the solidification front. The numerical model is calibrated to the experimental results, by selecting a characteristic bulk mean flow. In this case, experimental observations have shown the velocity ahead of the solidification front to be around 200μm/s. This velocity is comparable but larger than those observed and predicted in natural convection.

Figure 4 shows the transient evolution of the microstructure under the influence of forced convection. The numerical results show that as flow passes around and over a dendrite, solute is transported downstream forming an extended enriched region. The incident flow on a dendrite can have two effects which depend on the solute concentration transported. Incident flow that has been enriched after passing an upstream dendrite will stunt downstream dendrites. However, if the incident flow transports bulk material, then growth of both the primary tip and secondary arms will be promoted. This flow-dependent competition between neighbouring grains causes a significant increase in the primary arm spacing compared to the control case. Natural convection is still present and plumes of enriched solute are released into the bulk. However, due to bulk mean flow the plumes are transported downstream of the sample. These mechanisms are also observed experimentally with preferential growth of the secondary arms and an increase in the primary arm spacing clearly shown in figure 4.

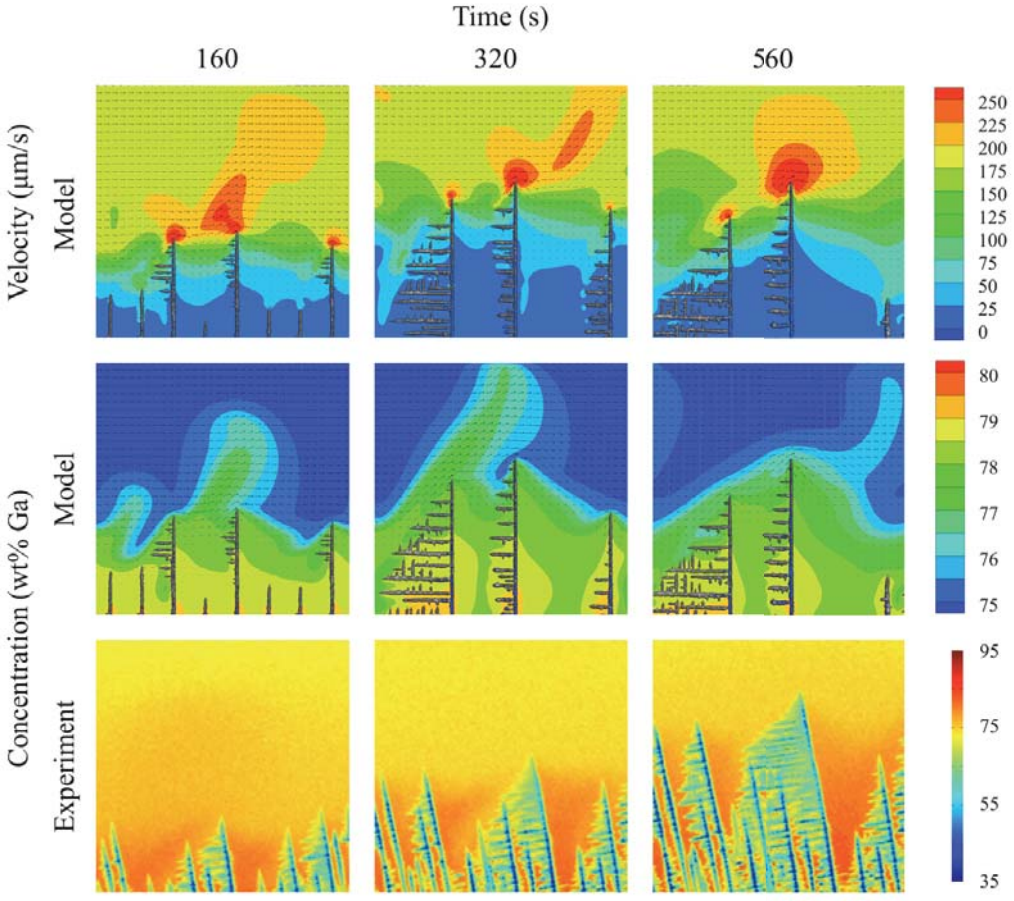

Figure 4. Transient evolution of microstructure under the influence of forced convection. Top: numerical model flow velocity. Middle: numerical model solute concentration. Bottom: experimental solute concentration

4.3 Thermoelectric magnetohydrodynamics

Figure 5 shows transient numerical results for the velocity, concentration and current density. The current passes up through the dendrites, emanating from the tips and then back down through the inter-dendritic liquid. Application of a 1T external magnetic field generates a Lorentz force, driving flow in inter-dendritic regions where there is a significant current. However as the porosity decreases the inter-dendritic flow becomes restricted. This creates a region of relatively high velocity that tracks the solidification front. The velocity is slower than the natural and forced convection cases, about half and a quarter respectively. However, the underlying mechanism is similar to forced convection, as this region of velocity transports liquid downstream. Depending on the concentration of the liquid, growth is either promoted or stunted. However, in contrast to the case of forced convection, the absence of currents in the bulk combined with electromagnetic damping gives no bulk mean flow. Moreover, electromagnetic damping slows the formation of plumes of solute, where after 360s the first plumes are only just emerging. In comparison to the case of only natural convection several plumes had formed and destabilised within this time scale. The inability to effectively eject solute into the bulk causes the inter-dendritic region to become more enriched compared to the other cases.

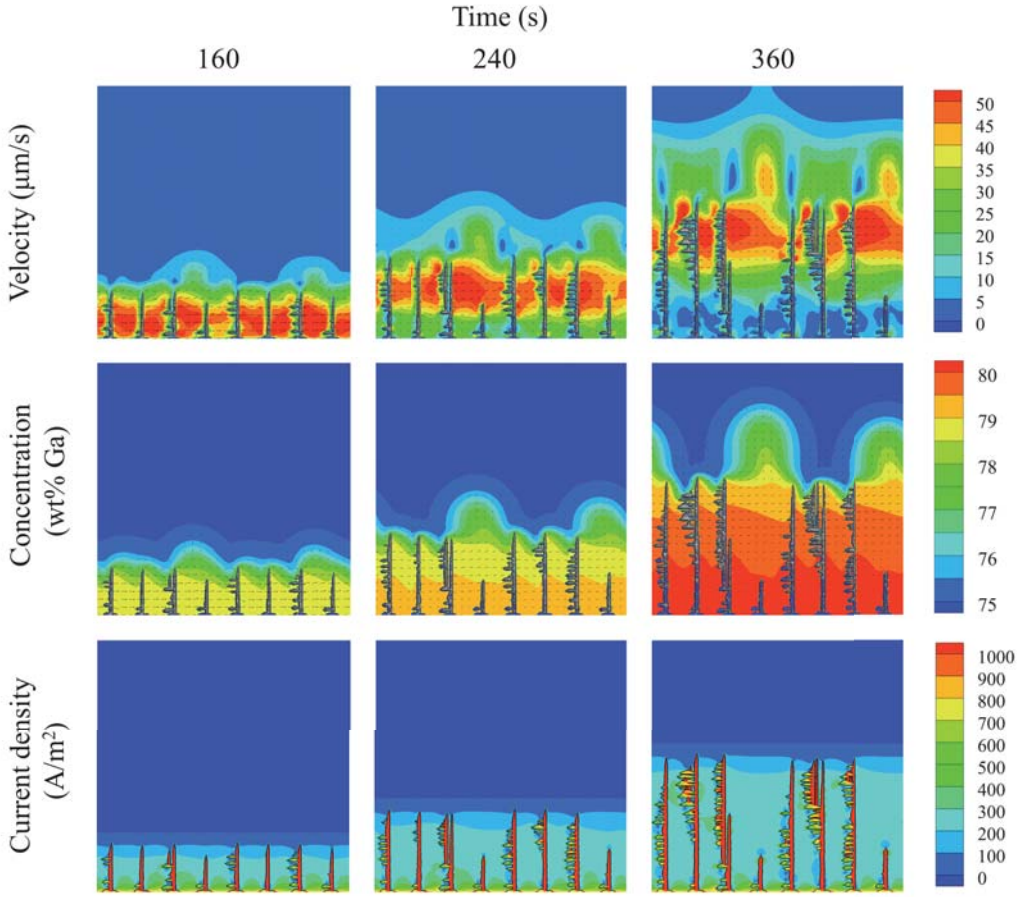

Figure 5. Numerical results for the transient evolution of microstructure under the influence of an external 1T DC magnetic field. Top: flow velocity. Middle: solute concentration. Bottom: current density.

5. Conclusion

The introduction of convection during solidification has been shown to have a significant impact on the evolution of the microstructure. The effects of natural, forced and thermoelectric magnetohydrodynamic convection during solidification of a Ga-In25%wt. thin sample were investigated. Natural convection is present in this system due to significant variations in density between the two components causing plumes of solute to be ejected into the melt. This mechanism was observed both experimentally and numerically.

Using a magnetic wheel, forced convection conditions were generated close to the solidification front. By using the observed bulk mean velocity an equivalent body force was calibrated for the numerical model. Both the numerical and experimental results of forced convection show that the microstructure exhibits preferential growth of secondary branches and an increase in primary arm spacing. These changes are caused by the downstream transport of solute. The final case investigated the effects of thermoelectric magnetohydrodynamics. Numerical simulations show similarities to the forced convection case, with inter-dendritic flow causing preferential growth of secondary arms. In the melt where there are no thermoelectric currents, the flow is dominated by electromagnetic damping. Consequently the formation of solute plumes is significantly slowed compared to the other cases.

Acknowledgments

The research is supported by the EPSRC (EPK011413/1) and the German Helmholtz Association in form of the Helmholtz-Alliance “LIMTECH”.

References

[1] Reed R C, Tao T and Warnken N 2009 *Acta Mater.* **57** pp 5898-5913
[2] Madison J, Spowart J, Rowenhorst D, Aagesen L K, Thornton K and Pollock T M 2010 *Acta Mater.* **58** pp 2864-2875
[3] Beckermann C, Gu J P and Boettinger W J 2000 *Metall. and Mater. Trans. A* **31A** pp 2545-2557
[4] Boden S, Eckert S, Gerbeth G 2010 *Mater Lett.* **64** pp 1340-1343
[5] Shevchenko N, Boden S, Gerbeth G and Eckert S 2013 *Metall. And Mat. Trans. A* **44** pp 3797-3808
[6] Boden S, Eckert S, Willers B and Gerbeth G 2008 *Metall. Mat. Trans. A* **39** pp 613-623
[7] Pericleous K A, Djambazov G Ward M, Yuan L and Lee P D (2013) *Metall and Mat Trans A* **44** (12) pp 5365-5376
[8] Guo, J, and Beckermann, C 2003 *Num Heat Transfer, A* **44**, pp 559-576
[9] Karagaddea S, Yuan L, Shevchenko N, Eckert S and Lee P D 2014 *Acta Mater.* **79** pp 168-180
[10] Voller V 2007 *Int J. Heat Mass Transfer* **51** pp 823-834
[11] Kao A and Pericleous K 2012 *J. Algor. Comp. Tech.* **(6)1** pp 173-201
[12] Kao A and Pericleous K 2012 *J. of Iron and Steel Research International* **(19)1** pp 317-321
[13] Kao A and Pericleous K 2012 *Modeling of Casting, Welding, and Advanced Solidification Processes - XIII (MCWASP XIII). IOP Conf. Series: Mat. Sci. Eng.* **33** 012045
[14] Kao A and Pericleous K 2012 *Magnetohydrodynamics* **(48)2** pp 361-370
[15] Kao A, Lee P D and Pericleous K 2014 *ISIJ International* **54(6)** pp 1283-1287
[16] Shercliff J A 1979 *J. Fluid Mech.* **(91)2** pp 231-251